Comparative Evaluation of Two Glycine Transporter 1 Radiotracers [^{11}C]GSK931145 and [^{18}F]MK-6577 in Baboons

MING-QIANG ZHENG,[1†] SHU-FEI LIN,[1†*] DANIEL HOLDEN,[1] MIKA NAGANAWA,[1] JIM R. ROPCHAN,[1] SOHEILA NAJAFZADEN,[1] MICHAEL KAPINOS,[1] MIKE TABRIZ,[1] RICHARD E. CARSON,[1] TERENCE G. HAMILL,[2] AND YIYUN HUANG[1]

[1]*Department of Radiology and Biomedical Imaging, Yale University School of Medicine, PET Center, New Haven, Connecticut*

[2]*Discovery Imaging, Merck Research Laboratories, West Point, Pennsylvania*

KEY WORDS PET imaging; GlyT1; [^{11}C]GSK931145; [^{18}F]MK-6577

ABSTRACT Glycine transporter type-1 (GlyT1) has been proposed as a target for drug development for schizophrenia. PET imaging with a GlyT1 specific radiotracer will allow for the measurement of target occupancy of GlyT1 inhibitors, and for *in vivo* investigation of GlyT1 alterations in schizophrenia. We conducted a comparative evaluation of two GlyT1 radiotracers, [^{11}C]GSK931145, and [^{18}F]MK-6577, in baboons. Two baboons were imaged with [^{11}C]GSK931145 and [^{18}F]MK-6577. Blocking studies with GSK931145 (0.3 or 0.2 mg/kg) were conducted to determine the level of tracer specific binding. [^{11}C]GSK931145 and [^{18}F]MK-6577 were synthesized in good yield and high specific activity. Moderately fast metabolism was observed for both tracers, with ~30% of parent at 30 min post-injection. In the brain, both radiotracers showed good uptake and distribution profiles consistent with regional GlyT1 densities. [^{18}F]MK-6577 displayed higher uptake and faster kinetics than [^{11}C]GSK931145. Time activity curves were well described by the two-tissue compartment model. Regional volume of distribution (V_T) values were higher for [^{18}F]MK-6577 than [^{11}C]GSK931145. Pretreatment with GSK931145 reduced tracer uptake to a homogeneous level throughout the brain, indicating *in vivo* binding specificity and lack of a reference region for both radiotracers. Linear regression analysis of V_T estimates between tracers indicated higher specific binding for [^{18}F]MK-6577 than [^{11}C]GSK931145, consistent with higher regional binding potential (BP_{ND}) values of [^{18}F]MK-6577 calculated using V_T from the baseline scans and non-displaceable distribution volume (V_{ND}) derived from blocking studies. [^{18}F]MK-6577 appears to be a superior radiotracer with higher brain uptake, faster kinetics, and higher specific binding signals than [^{11}C]GSK931145. **Synapse 70:112–120, 2016.**

INTRODUCTION

The glycine transporter-1 (GlyT1) is a member of the Na^+/Cl^--dependent transporter family and modulates the local concentrations of glycine, which is a coagonist with *D*-serine at the *N*-methyl-*D*-aspartate (NMDA) receptors. Inhibition of GlyT1 leads to an increase in cerebral glycine concentration and improvements in negative symptoms and cognitive deficits of patients with schizophrenia (see (Javitt, 2012) for review). The beneficial effects of treatment with sarcosine, a GlyT1 inhibitor, on the symptoms of schizophrenic patients were also concluded from a recently published phase III study (Strzelecki et al., 2015).

In the past few years, many efforts have been made to develop GlyT1 inhibitor positron emission tomography (PET) radioligands to probe the pathophysiology of diseases such as schizophrenia and to aid in the development of novel, GlyT1-targeting therapeutic agents (Fig. 1). Among these GlyT1 specific PET radioligands,

Ming-Qiang Zheng and Shu-fei Lin contributed equally to this work.

**Correspondence to*: Shu-fei Lin, Yale PET Center, PO Box 208048 801 Howard Avenue New Haven, CT 06520. E-mail: Shu-fei.lin@yale.edu

Received 17 October 2015; Revised 2 December 2015; Accepted 11 December 2015

DOI: 10.1002/syn.21879

Published online 6 January 2016 in Wiley Online Library (wileyonlinelibrary.com).

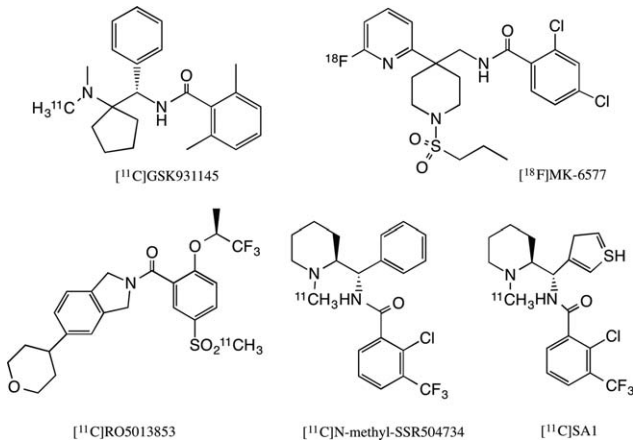

Fig. 1. Structures of selected GlyT1 radioligands.

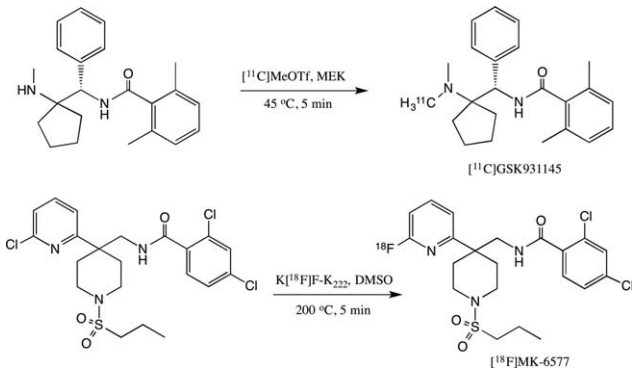

Fig. 2. Radiosynthesis of [^{11}C]GSK931145 and [^{18}F]MK-6577.

[^{11}C]GSK931145, [^{18}F]MK-6577, and [^{11}C]RO5013853 have shown promise in preclinical and clinical evaluations (Gunn et al., 2011; Joshi et al., 2015; Wong et al., 2013). Others, such as [^{11}C]*N*-methyl-SSR504734 and [^{11}C]SA1, have also demonstrated their potential in imaging GlyT1 in nonhuman primates (Fuchigami et al., 2012; Toyohara et al., 2011).

[^{11}C]GSK931145 was the first GlyT1 PET tracer successfully used to quantify the transporter occupancy achieved by GlyT1 inhibitors in animal models (Castner et al., 2014; Gunn et al., 2011; Passchier et al., 2010), as well as in clinical trials in healthy human subjects (Gunn et al., 2011). Several good characteristics of this radiotracer were noted, including good brain penetration, heterogeneous tissue binding displaceable by selective GlyT1 inhibitors, and acceptable pharmacokinetics (Gunn et al., 2011; Passchier et al., 2010). Another radiotracer, [^{18}F]MK-6577, was first reported by Hamill et al. (Hamill et al., 2011) in rhesus monkeys to have good brain uptake, specific binding to brain regions with high GlyT1 concentrations, and reversible tissue binding kinetics. Initial results from a human study also indicated the suitability of [^{18}F]MK-6577 as a PET radiotracer to measure the brain penetration and transporter occupancy of candidate drugs in humans (Joshi et al., 2015). A third GlyT1 radiotracer, [^{11}C]RO5013853, was evaluated in baboons and humans, and appeared to be suitable for measuring engagement of bitopertin with GlyT1, and the optimal inhibition/occupancy associated with a positive effect on cognition was found to be in the $50 \pm 20\%$ range (Martin-Facklam et al., 2013; Wong et al., 2013).

In the present study, we compared the pharmacokinetic and imaging characteristics of [^{11}C]GSK931145 and [^{18}F]MK-6577 in baboons. The purpose was to identify an optimal GlyT1 radiotracer for use in clinical research to measure the potential GlyT1 alterations in neuropsychiatric disorders, and to determine the relationship among dose, plasma exposure, target engagement and therapeutic efficacy of GlyT1 inhibitors.

MATERIALS AND METHODS

Synthesis of [^{11}C]GSK931145

[^{11}C]GSK931145 was synthesized with a GE FXC automated module by bubbling [^{11}C]MeOTf into a solution of the desmethyl precursor (0.5 – 0.8 mg) in anhydrous methylethyl ketone (MEK, 0.3 mL). After the radioactivity peaked, the resulting mixture was heated for 5 min at 45 °C (Fig. 2) and purified by semi-preparative HPLC with a Phenomenex Prodigy C18 column (10 × 250 mm, 10 μm, Torrance, CA) eluting with a mobile phase of 40% acetonitrile and 60% 0.1 M ammonium acetate with 0.1% acetic acid (v/v, pH = 5.5) at a flow rate of 5 mL/min. The product fraction eluting at 12–14 min was collected and diluted in a solution of 200 mg ascorbic acid in 50 mL of deionized water (DI). The solution was then passed through a Waters Classic C18 SepPak cartridge. The SepPak was rinsed with 0.01 N HCl (10 mL) and dried. The trapped product was eluted off the SepPak with 1 mL of absolute ethanol (U.S. Pharmacopeial Convention, USP grade) followed by 3 mL of USP saline into a product vial containing 7 mL of USP saline and 40 μL of 4.2% USP Na_HCO_3 solution. The mixture was then passed through a sterile membrane filter (0.22 μm, Millipore) and collected in an empty sterile vial to afford a formulated solution ready for injection.

Quality control tests to determine the radiochemical purity, specific activity, and identity of the final product were performed on a Phenomenex Prodigy analytical column (4.6 × 250 mm, 5 μm) eluting with a mobile phase of 40% acetonitrile and 60% 0.1 M ammonium formate (v/v) at a flow rate of 2.0 mL/min.

Synthesis of [^{18}F]MK-6577

[^{18}F]MK-6577 was synthesized using a homemade semi-automated module. [^{18}F]fluoride in [^{18}O]water was trapped with a QMA cartridge and then eluted off by a solution of Kryptofix 222/K_2CO_3 (1.4 mL, 10

mg of Kryptofix 222 dissolved in 1.0 mL acetonitrile and 2.6 mg of potassium carbonate dissolved in 0.4 mL water) into a 2 mL v-vial. The solution was first dried at 105°C for 10 min under a steam of argon, followed by the addition of two portions of 0.4 mL MeCN each. Azeotropic drying continued for another 5–10 min. A solution of the precursor in DMSO (0.2 mL) was then added and the mixture heated at 200°C for 5 min (Fig. 2). The resulting solution was cooled, diluted with 1.5 mL of 50:50 MeCN/0.1% trifluoroacetic acid (TFA) (v/v), and loaded onto a Phenomenex Luna C18(2) column (10 × 250 mm, 10 μm) eluting with a mobile phase of 50% acetonitrile in 0.1% TFA (v/v) at a flow rate of 5 mL/min. The product fraction eluting at 17–18 min was collected, diluted with DI water (50 mL with 400 mg of ascorbic acid), and passed through a Waters Classic C18 SepPak cartridge. The SepPak was rinsed with 0.01 N HCl (10 mL) and dried. The product was then eluted off with 1 mL of absolute ethanol (USP grade), followed by a solution of 3 mg ascorbic acid in 3 mL of USP saline, into a 10 mL syringe barrel pre-loaded with 7 mg of ascorbic acid and 200 μL of 4.2% $NaHCO_3$ in 7 mL of USP saline. The formulated mixture was then passed through a sterile membrane filter (0.22 μm) into a sterile dose vial.

Quality control analyses were performed on an analytical HPLC system equipped with a Phenomenex Luna C18(2) column (4.6 × 250 mm, 5 μm) and eluting with a mobile phase of 52% acetonitrile and 48% 0.1 M ammonium formate (v/v) at a flow rate of 2.0 mL/min to determine radiochemical purity, chemical purity, and specific activity of the final [^{18}F]MK-6577 solution. Identity of the product was confirmed by co-injection of the product solution with authentic MK-6577 standard, and co-elution of the UV and radioactive peak.

Lipophilicity measurements

An aliquot of the radioligand solution (~740 kBq) was added to a 2.0 mL microtube containing 0.8 mL of 1-octanol and 0.8 mL of 1 × Dulbecco's phosphate buffered saline (PBS, pH= 7.4). The mixture was vigorously vortexed for 20 s and centrifuged at 2,000 *g* for 2 min. A subsample of the 1-octanol (0.2 mL) and PBS (0.7 mL) layers was counted with a gamma well counter (Wizard 1480/2480, Perkin Elmer, Waltham, MA). The major portion of the 1-octanol layer (0.5 mL) was then diluted with 0.3 mL of 1-octanol and mixed with a fresh portion of 0.8 mL PBS. Six consecutive equilibrations were performed for each radioligand. An equal volume of 1-octanol and aqueous layer after the last equilibration was counted. Partition coefficient was determined as the ratio of activity in 1-octanol to that in the aqueous phase.

PET imaging procedures in baboons

Two female baboons (Papio, age of 5.7 and 8 years and weight of 22.8 and 12.8 kg, respectively) were used in the PET imaging studies. Experiments in animals were performed in accordance with a protocol approved by the Yale Institutional Animal Care and Use Committee.

Baboons were first sedated with ketamine hydrochloride (10 mg/kg) intramuscularly ~2 h prior to the initiation of PET scans, and then maintained on oxygen and 1.5 − 3.0% isoflurane. Vital signs including respiration rate, blood pressure, heart rate, and temperature were monitored continuously and recorded every 15 min, and temperature was kept constant at 37°C with heated water blankets. PET scans were performed on the HR+ PET scanner (Siemens/CTI, Knoxville, TN), with an intrinsic image resolution of 5 mm. Following a 6-min transmission scan (for attenuation correction), [^{11}C]GSK931145 (137 ± 35 MBq, 0.012 ± 0.006 μg/kg, $n = 6$) or [^{18}F]MK-6577 (110 ± 63 MBq, 0.063 ± 0.09 μg, $n = 4$) was administered as a 3-minute slow bolus using a syringe pump (Harvard PHD 22/2000; Harvard Apparatus, Holliston, MA), and emission data were acquired for 120 and 180 min, respectively. For blocking experiments, GSK931145 (0.3 or 0.2 mg/kg) was administered as a 10-min infusion, initiated 10–20 min before the injection of the radiotracer.

Metabolite analysis and arterial input function measurement

The arterial plasma input functions corrected for the presence of radiometabolites were generated for all scans based on blood samples taken from the femoral artery. Sequential blood samples (0.5–5 mL) were collected manually at 21 selected time-points during the entire scan and plasma was separated from blood cells by centrifugation (2,930 *g* for 5 min at 4°C; Allegra X-22R Centrifuge, Beckman Coulter, Fullerton, CA). Whole blood and plasma samples were counted with cross-calibrated gamma well counters.

Arterial plasma samples obtained at 3, 6, 15, 30, 60, and 90 min post-injection of [^{11}C]GSK931145 and 3, 8, 15, 30, 60, 90, 120, 180 min after [^{18}F]MK-6577 injection were treated with urea (8 M) and filtered through 1.0 μm Whatman 13 mm GD/X syringe filters (GE, Florham Park, NJ) for metabolite analysis. Up to 5 mL of plasma filtrate was injected onto an automatic column-switching HPLC system equipped with a capture column (19 × 4.6 mm) packed with Phenomenex SPE Strata-X sorbent (Torrance, CA, USA) and eluting with 1% acetonitrile in water at a flow rate of 2 mL/min. After 4 min, activity trapped on the capture column was back-eluted onto a Phenomenex Gemini-NX analytical column (5 μm, 4.6 × 150 mm) with a mobile phase of 35% acetonitrile and 65% 0.1 M ammonium formate (v/v) at a flow

rate of 1.8 mL/min for the determination of unchanged fractions of [^{11}C]GSK931145. For [^{18}F]MK-6577, a Phenomenex Luna C18(2) analytical column (5 μm, 4.6 × 250 mm) was used and eluted with a mobile phase of 60% acetonitrile and 40% 0.1 M ammonium formate (v/v) at a flow rate of 1.5 mL/min. The unmetabolized parent fraction was determined as the ratio of the radioactivity corresponding to the parent (retention time of ~11 min for both tracers) to the total amount of radioactivity collected, and fitted with an inverted gamma or a bounded sum of exponentials function for [^{11}C]GSK931145 and [^{18}F]MK-6577, respectively. The arterial plasma input function was calculated as the product of the plasma time-activity curve (TAC) and the parent fraction curve.

Plasma free fraction (f_P) was measured with the ultrafiltration method using Millipore Centrifree® micropartition devices (4104, Billerica, MA) with 3 mL of arterial blood taken immediately prior to the PET tracer injection and spiked with ~10 kBq of [^{11}C]GSK931145 or [^{18}F]MK-6577 product solution. The f_P was determined as the radioactivity ratio of ultrafiltrate to plasma.

Image analysis and kinetic modeling

Regions of interest (ROIs) in the brain were determined from a baboon atlas with registration of each animal's MR scan to the atlas, followed by registration of the PET images to the animal's MR to generate regional time activity curves (TACs). Outcome measures were derived with kinetic analysis of the regional TACs using the metabolite-corrected arterial plasma TAC as the input function. One- and two-tissue compartment (1TC, 2TC) models were applied to TACs to calculate the regional total volume of distribution (V_T) (Innis et al., 2007). For the blocking experiments with GSK931145, target occupancy and nondisplaceable distribution volume (V_{ND}) were calculated with V_T values from the baseline and blocking scans using the occupancy plot (Cunningham et al., 2010). Given a lack of reference region (see Results), binding potential (BP_{ND}) was calculated as $BP_{ND} = (V_T - V_{ND})/V_{ND}$ (unitless) using the V_{ND} values derived from the occupancy plots. To compare the specific binding of [^{11}C]GSK931145 and [^{18}F]MK-6577, linear regression analysis was performed using V_T estimates from 12 different brain regions according to the method of Guo et al. (2014). In addition, with the values of plasma free fraction (f_p) measured for the two tracers in this study and the measured in vivo affinity (K_d) of 1.87 nM as recently reported for [^{18}F]MK-6577 (Xia et al., 2015), the in vivo K_d of [^{11}C]GSK931145 was also determined from the slope of the regression line (slope = $f_{P\ [^{11}C]GSK931145}$ * $K_{d\ [^{18}F]MK\text{-}6577}/f_{P\ [^{18}F]MK\text{-}6577}/K_{d\ [^{11}C]GSK931145}$) (Guo et al., 2014).

RESULTS

Radiosynthesis

[^{11}C]GSK931145 and [^{18}F]MK-6577 were successfully synthesized with sufficient quantity and quality for baboon study. For [^{11}C]GSK931145, radiochemical yield was 6.56 ± 3.76% (decay-uncorrected, based on activity of trapped [^{11}C]MeOTf), with specific activity of 973.1 ± 584.6 MBq/nmol at the end of synthesis (EOS, $n = 14$). Radiochemical purity was >95%. For [^{18}F]MK-6577, radiochemical yield was 20.8 ± 3.8% (decay-uncorrected, based on [^{18}F]fluoride), with specific activity of 547.6 ± 403.3 MBq/nmol (EOS, $n = 10$). Radiochemical purity was > 99%.

Comparison of [^{11}C]GSK931145 and [^{18}F]MK-6577 in baboons

Plasma analysis and log P measurement

Analysis of arterial plasma following tracer administration revealed the formation of three to four radiometabolites (Figs. 3A and 3B). Given the shorter retention times of the metabolite peaks than the parent on the gamma HPLC chromatograms, all radiolabeled metabolite species appeared more hydrophilic than the parent. The metabolite-corrected plasma TACs and parent fraction over time of [^{11}C]GSK931145 and [^{18}F]MK-6577 are shown in Figures 3C–3F. In the baseline scans, both tracers displayed similar rates of metabolism, with ~30% parent fraction in plasma at 30 min post-injection. Pretreatment with GSK931145 appeared to have no effect on tracer metabolism. The plasma free fraction in baboons was higher for [^{18}F]MK-6577 (16.0 ± 5.1%, $n = 4$) than [^{11}C]GSK931145 (5.3 ± 2%, $n = 6$). The measured log P values were 2.63 ± 0.11 and 3.06 ± 0.19, respectively, for [^{11}C]GSK931145 and [^{18}F]MK-6577 ($n = 9$ measurements each).

Brain analysis

Regional TACs from the baseline and blocking scans of [^{11}C]GSK931145 and [^{18}F]MK-6577 are presented in Figure 4 and PET images in Figure 5. Both [^{11}C]GSK931145 and [^{18}F]MK-6577 entered into the baboon brain rapidly, with concentrations of radioactivity peaking in most brain regions within 30 min post-injection. Heterogeneous distribution of these two tracers in the brain was observed. The highest uptake was seen in the brain stem and pons, followed by cerebellum, thalamus, and putamen, and lowest in cortical regions. Peak uptake of [^{18}F]MK-6577 (SUV of ~4) was higher than that of [^{11}C]GSK931145 (SUV of ~1.8). [^{18}F]MK-6577 displayed fast kinetics, with uptake in all regions peaking within 10 min after injection and clearing rapidly, while the tissue kinetic profile for [^{11}C]GSK931145 was more protracted (slower uptake and wash-out). Following pretreatment with GSK931145, uptake of both tracers was reduced to a homogeneous level throughout the brain,

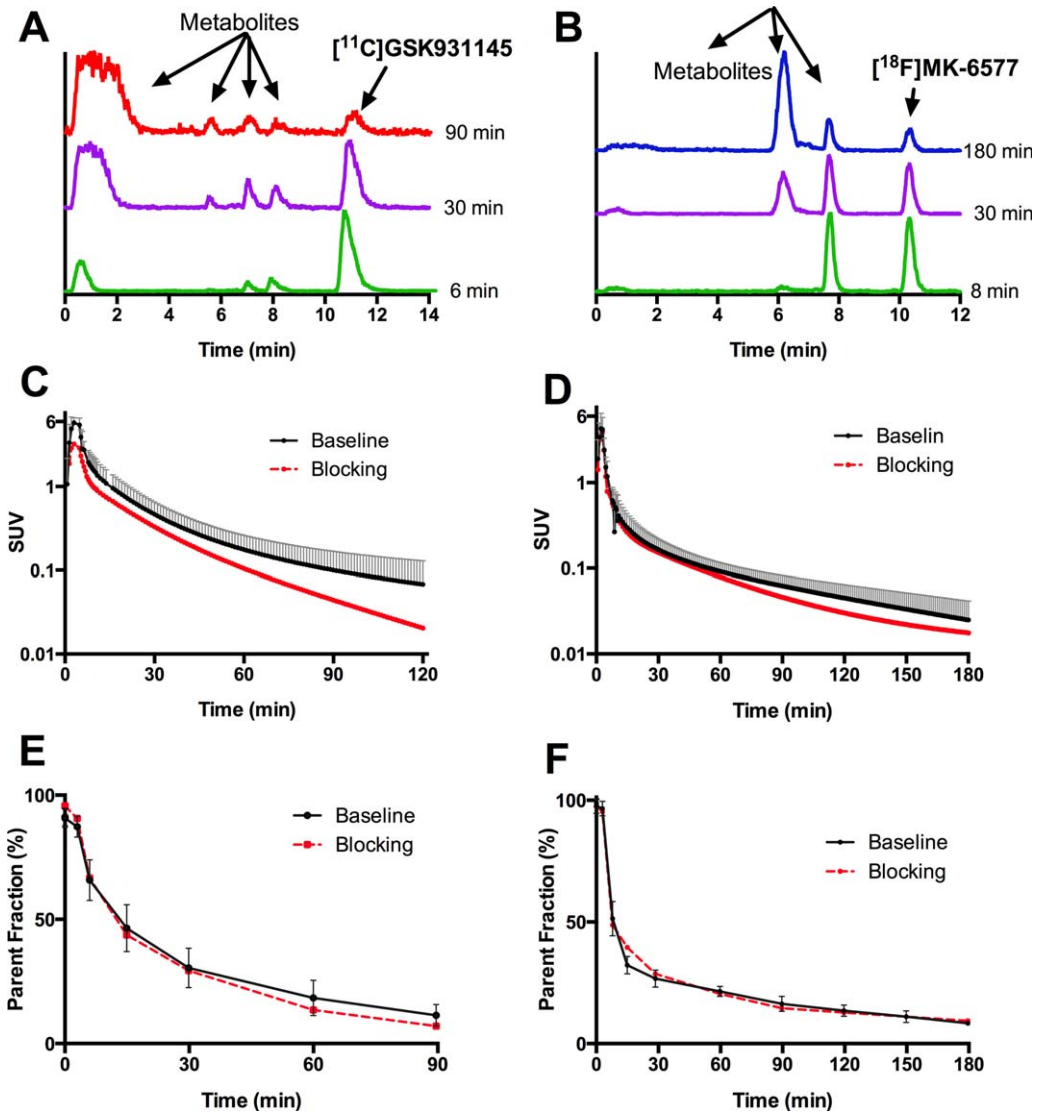

Fig. 3. HPLC chromatograms from plasma metabolite analysis of [^{11}C]GSK931145 (A) and [^{18}F]MK-6577 (B) at different time points; Mean ± S.D. of metabolite-corrected plasma time-activity curves on a logarithmic scale and percentage of parent fraction in plasma over time for [^{11}C]GSK931145 (C, E) and [^{18}F]MK-6577 (D, F) during baseline ($n = 5$ for [^{11}C]GSK931145; $n = 3$ for [^{18}F]MK-6577) and blocking scans ($n = 1$ each). Plasma curves are displayed in SUV units [concentration/(injected dose/body weight)].

indicating blockade of specific binding by the drug (Fig. 5) and implying the lack of a reference tissue devoid of specific binding.

Baseline TACs were analyzed with 1TC and 2TC models using the metabolite-corrected plasma TAC as input function. Based on the F-test results, the 2TC model was better than the 1TC model in all regions. Regional V_T values estimated with 2TC model are listed in Table I.

Pretreatment with GSK931145 reduced V_T in all regions for both [^{11}C]GSK931145 and [^{18}F]MK-6577 (Table I), confirming the lack of a reference region for these two GlyT1 radiotracers. Transporter occupancy by GSK931145 was estimated from the slope of the occupancy plot regression lines (Cunningham et al., 2010). GSK931145 at a dose of 0.3 mg/kg occupied 98% of GlyT1 when measured with [^{11}C]GSK931145, while the blocking study with [^{18}F]MK-6577 showed 77% occupancy with 0.2 mg/kg of GSK931145. The non-displaceable distribution volume (V_{ND}), obtained from the intercept of the occupancy plot, was 2.18 mL·cm^{-3} for [^{11}C]GSK931145 and 1.96 mL·cm^{-3} for [^{18}F]MK-6577. Using the V_{ND} values derived from the occupancy plots, regional estimates of binding potential (BP_{ND}) were calculated as $BP_{ND} = (V_T - V_{ND})/V_{ND}$ (unitless), and ranged from 0.9 to 3.9 for [^{18}F]MK-6577 and 0.5 to 1.3 for [^{11}C]GSK931145 in baboons (Table I).

Result from the graphical analysis of [^{11}C]GSK931145 and [^{18}F]MK-6577 V_T is shown in Figure 6. The simple

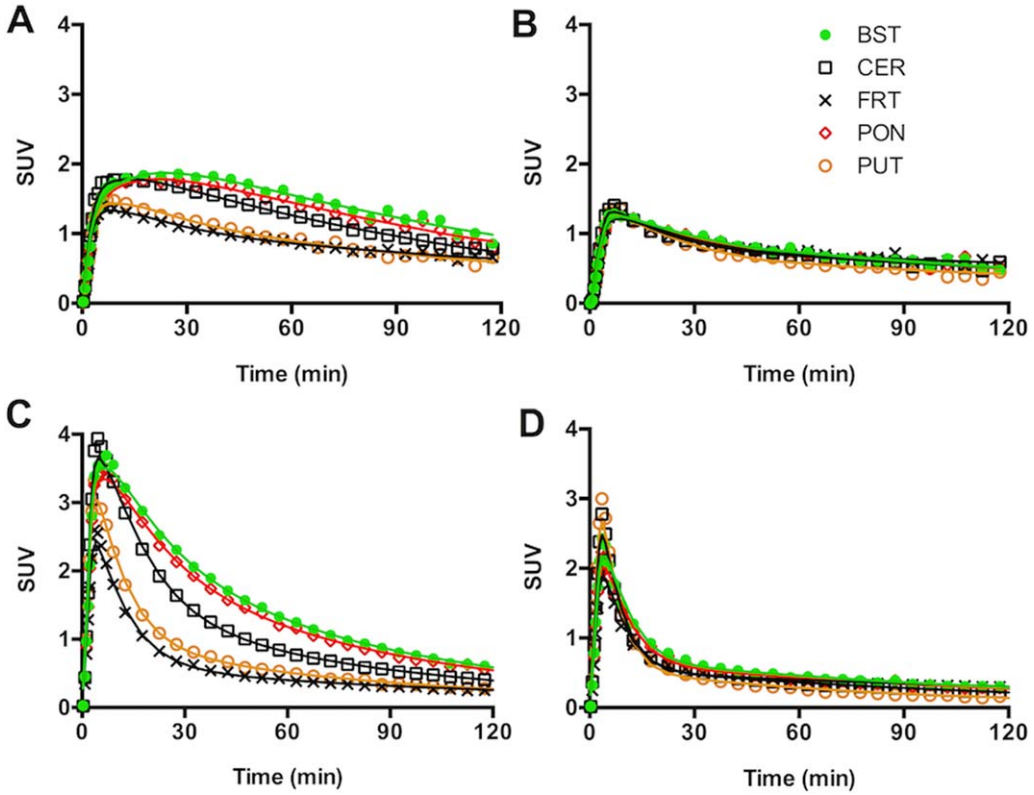

Fig. 4. Time-activity curves of [^{11}C]GSK931145 (A: baseline scan; B: blocking scan with 0.3 mg/kg GSK931145) and [^{18}F]MK-6577 (C: baseline scan; D: blocking scan with 0.2 mg/kg GSK931145) in selected baboon brain regions with 2TC fits. BST: brain stem, CER: cerebellum, FRT: frontal cortex, PON: pons, PUT: putamen. Radioactivity concentrations are expressed as SUV (concentration/(injected dose/body weight)).

linearity of the regression with $R^2 = 0.96$ indicates that the two radiotracers indeed bind to the same target in the baboon brain (Guo et al., 2014). The positive y-intercept identifies [^{18}F]MK-6577 as having higher specific binding (BP_{ND}), i.e., higher specific-to-nonspecific binding ratio *in vivo*, than [^{11}C]GSK931145. This conclusion is in agreement with results shown in Table I: higher regional BP_{ND} values were found for [^{18}F]MK-6577, as calculated using regional V_T values from the baseline scans and V_{ND} derived from the blocking studies in the same baboon. Given the slope of 0.321 for the regression line in Figure 6, plasma free fraction of 16% for [^{18}F]MK-6577 and 5.3% for [^{11}C]GSK931145 from this study, and $K_d = 1.87$ nM for [^{18}F]MK-6577 as reported recently (Xia et al., 2015), the *in vivo* K_d of [^{11}C]GSK931145 as derived as 1.93 nM. In another word, using this linear regression analysis, we could deduce similar binding affinities of [^{18}F]MK-6577 than [^{11}C]GSK931145 for GlyT1 in the baboon brain.

DISCUSSION

The GlyT1 has been proposed as a target for drug development in schizophrenia. PET imaging with GlyT1 specific radiotracer is a tool for measuring the dose-exposure-target occupancy relationship of emerging GlyT1-targeted therapeutic agents, and for *in vivo* investigation of the GlyT1 in patients with schizophrenia. As a result, a large amount of effort has been made to develop suitable GlyT1 imaging agents for use in humans, and three leading molecules were proposed as promising GlyT1 PET radiotracers (Fig. 1). In this study we conducted a side-by-side comparison of two radiotracers, [^{11}C]GSK931145 and [^{18}F]MK-6577, in baboons to assess their pharmacokinetics, specific binding profiles, and overall imaging properties. The goal was to select the optimal radiotracer for use in our PET imaging studies in humans.

[^{11}C]GSK931145 and [^{18}F]MK-6577 were successfully produced in good radiochemical yield and purity. A fully automated method with less amount of precursor (0.5 − 0.8 mg vs.1 mg) in MEK (instead of acetone) and higher reaction temperature (45 °C vs. 30 °C) was used for radiosynthesis of [^{11}C]GSK931145, as compared with conditions reported in the literature (Passchier et al., 2010). Previous radiosynthesis of [^{18}F]MK-6577 used microwave heating at 75 W and 140 °C for 3 min (Hamill et al., 2011). We used conventional heating for this radiolabeling and found that at this temperature very low radiochemical yield was obtained (<10% of incorporation yield

at 140 or 160 °C). By raising the reaction temperature to 200 °C with reaction time of 5 min, we were able to significantly improve the radiochemical yield and specific activity of [^{18}F]MK-6577. Decay-uncorrected radiochemical yield was 20.8 ± 3.8% (n = 10) in this study, as compared with 6.4 ± 1.0% reported in the literature (Hamill et al., 2011). Specific activity at end of synthesis was 547.6 ± 403.3 GBq/mmol, compared with 95.5 ± 23.1 GBq/mmol in the literature. Radiochemical and chemical purity of the [^{18}F]MK-6577 final product was > 99%.

The measured log P values, as an indicator of a compound's lipophilicity, was 2.63 for [^{11}C]GSK931145 and 3.06 for [^{18}F]MK-6577. These values are in good agreement with measurements using the unlabeled compounds (log P of 2.53 for GSK931145 and 2.9 for MK-6577) (Hamill et al., 2011; Passchier et al., 2010). In baboons, both [^{11}C]GSK931145 and [^{18}F]MK-6577 displayed similar rates of metabolism, with ~30% parent fraction in plasma at 30 min post-injection. [^{18}F]MK-6577 had higher plasma free fraction (16.0 ± 5.1%, n = 4) in baboons than [^{11}C]GSK931145 (5.3 ± 2%, n = 6). This is somewhat surprising, given the higher log P values of [^{18}F]MK-6577 (3.06) compared with [^{11}C]GSK931145 (2.63). In general, higher log P value of a radiotracer is associated with lower plasma free fraction. It is not clear what causes the lower plasma free fraction for [^{11}C]GSK931145, but its behavior in plasma is somewhat peculiar compared to other radiotracers (see discussion below).

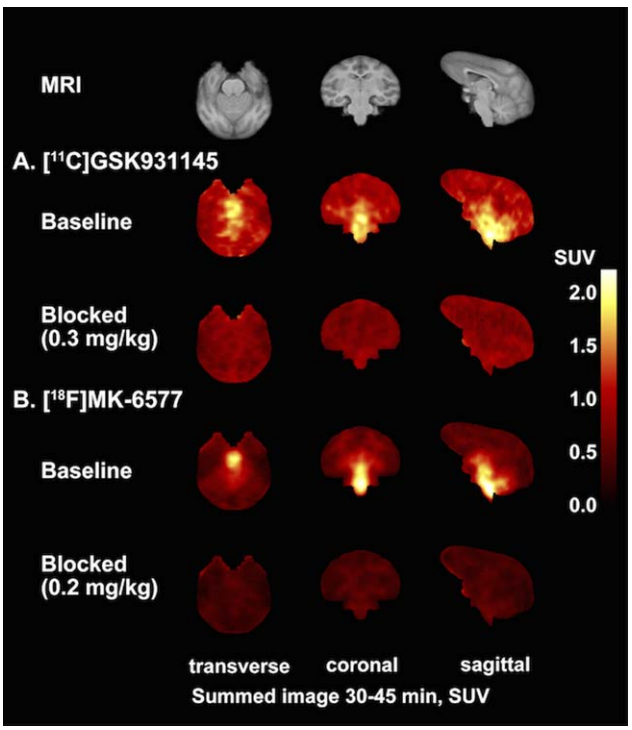

Fig. 5. SUV images summed from 30 to 45 min post-injection of [^{11}C]GSK931145 (A) and [^{18}F]MK-6577 (B) in coronal (left), transverse (middle) and sagittal (right) views, along with co-registered MR images (top).

PET imaging studies showed that both [^{11}C]GSK931145 and [^{18}F]MK-6577 readily enter into the brain with a heterogeneous distribution consistent with GlyT1 density profile (brain stem ~ pons ~ thalamus ~ cerebellum > cortex) and distribution patterns reported in previous publications in rhesus monkeys and humans (Gunn et al., 2011; Joshi et al., 2015; Passchier et al., 2010; Sanabria-Bohorquez et al., 2012). Brain uptake is faster and higher for [^{18}F]MK-6577 (peak SUV of ~4) than [^{11}C]GSK931145 (peak SUV of ~1.8) and the clearance is faster, i.e., overall faster tissue kinetics for [^{18}F]MK-6577 in baboons. Regional uptake levels were similar between baboons (this study) and humans (Gunn et al., 2011; Joshi et al., 2015) for both tracers, but the peak uptake level of [^{18}F]MK-6577 was higher in baboons (SUV ~4) than that in rhesus monkeys (SUV ~3) (Hamill et al., 2011; Sanabria-Bohorquez et al., 2012). Time-activity curves of the two tracers were fitted better with the 2TC than the 1TC model. The 2TC model was chosen for analysis based on the F-test, and consistent with the selection of kinetic model for both tracers in humans (Gunn et al., 2011; Joshi et al., 2015; Passchier et al., 2010; Sanabria-Bohorquez et al., 2012). Regional V_T values were reliably estimated with low standard errors (mean of 13%) by the 2TC model for both radiotracers. In comparison, [^{18}F]MK-6577 has higher regional V_T values than [^{11}C]GSK931145.

TABLE I. Regional 2TC V_T (mL·cm^{-3}) and BP_{ND} values of [^{11}C]GSK931145 and [^{18}F]MK-6577 in the baboon brain from the baseline scans (n = 2 each), and blocking scans with GSK931145 (n = 1 each)

	[^{11}C]GSK931145			[^{18}F]MK-6577		
Region	V_T Baseline (n = 2)	V_T Blocking (0.3 mg/kg)	Baseline BP_{ND}[a]	V_T Baseline (n = 2)	V_T Blocking (0.2 mg/kg)	Baseline BP_{ND}[a]
Brainstem	4.70 ± 0.76	2.39	1.32	9.04 ± 0.77	3.80	3.90
Cerebellum	3.57 ± 0.60	2.31	0.95	6.45 ± 0.24	3.06	2.39
Frontal Cortex	3.09 ± 0.52	2.66	0.95	4.19 ± 0.72	4.24	1.40
Occipital Cortex	2.65 ± 0.47	2.19	0.62	3.58 ± 0.33	2.49	0.95
Pons	4.31 ± 0.63	2.38	1.10	8.44 ± 0.73	3.51	3.58
Putamen	2.85 ± 0.54	2.14	0.87	4.22 ± 0.11	2.34	1.19
Thalamus	4.18 ± 0.64	2.08	1.00	6.02 ± 0.54	3.25	2.28

[a] $BP_{ND} = (V_T - V_{ND})/V_{ND}$.

Uptake of [^{18}F]MK-6577 and [^{11}C]GSK931145 was reduced substantially in all brain regions following administration of GSK931145, indicating the binding specificity of the two radiotracers. The reduced uptake in all brain regions also indicates the lack of a reference tissue devoid of specific binding. Because GlyT1 is present on both neuronal and glial cells throughout the mammalian brain (Cubelos et al., 2005), it is not surprising that binding blockade by GSK931145 was observed in all regions of the brain for both tracers, and a suitable reference region lacking GlyT1 binding could not be identified, a finding consistent with published data (Gunn et al., 2011; Hamill et al., 2011). The V_{ND} value, obtained from the intercept of the occupancy plot, is lower than the V_T value in any brain region, thus the lack of a reference region for either tracer is quantitatively affirmed. Using the V_{ND} value derived from the blocking scans, regional estimates of BP_{ND} were calculated: regional BP_{ND} is higher for [^{18}F]MK-6577 than [^{11}C]GSK931145 by 1.3 to 3.2 times in the baboon brain (Table I). In addition, the regression analysis indicates comparable binding affinity (K_d = 1.93 and 1.87 nM for [^{11}C]GSK931145 and [^{18}F]MK-6577, respectively) of both tracers for GlyT1 in the baboon brain, which is in good agreement with *in vitro* inhibition constants (K_i) in the literature: 1.15 nM for [^{18}F]MK-6577 in human brainstem homogenates (Hamill et al., 2011) and 1.07 nM for [^{11}C]GSK931145 in rat cortex homogenates (Passchier et al., 2010).

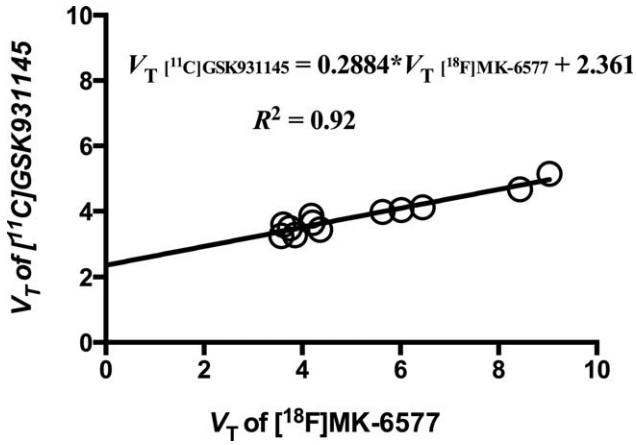

Fig. 6. Linear regression analysis of regional V_T between [^{11}C]GSK931145 and [^{18}F]MK-6577 in baboons.

Both [^{11}C]GSK931145 and [^{18}F]MK-6577 have been evaluated in rhesus monkeys (Gunn et al., 2011; Sanabria-Bohorquez et al., 2012), baboons (this study) as well as in humans (Gunn et al., 2011; Joshi et al., 2015). Table II summarizes the regional V_T and f_P values in different species. Regional V_T estimates of [^{11}C]GSK931145 in non-human primates were in a sharp contrast to those in humans, with a drop of >80% on average, while the V_T decreases were more modest for [^{18}F]MK-6577 from non-human primates to humans, averaging ~46%. These reductions in V_T values are paralleled by the decreases in plasma free fraction (f_P) of the radiotracers: f_P of [^{11}C]GSK931145 decreases from 8.0% in rhesus monkeys and 5.3% in baboons to 0.8% in humans (Gunn et al., 2011), while f_P of [^{18}F]MK-6577 changes from 16% in baboons to 6.8% in humans (unpublished data). It appears that the key driver for reduced regional V_T values of both radiotracers was the lower f_P values detected in humans. As noted before (Gunn et al., 2011), when V_T is normalized by f_P, the values are more stable and in agreement across different species as they reflect the partition coefficient with free tracer in plasma. However, the high test-retest variability of [^{11}C]GSK931145 in humans may restrict its utility for measuring population differences in GlyT1 availability.

In this study, we compared the pharmacokinetics and imaging characteristics of two GlyT1 radiotracers, [^{11}C]GSK931145 and [^{18}F]MK-6577, in baboons. Metabolism was similar for both radiotracers, but [^{18}F]MK-6577 had higher plasma free fraction. In the brain [^{18}F]MK-6577 displayed higher uptake levels

TABLE II. Regional V_T estimated from 2TC model and f_P of [^{11}C]GSK931145 and [^{18}F]MK-6577 in different species.

	[^{11}C]GSK931145			[^{18}F]MK-6577		
	Rhesus monkey[a] n=8	Baboon n=5	Human[a] n=10	Rhesus monkey[b] n=5	Baboon n=3	Human n=3
Region	V_T (mL·cm^{-3})					
Midbrain	4.87	4.70	0.79	5.80	9.04	5.50[c]
Thalamus	4.55	4.18	0.75	4.94	6.02	4.80[c]
Cerebellum	4.34	3.57	0.71	4.60	6.45	4.92[c]
Cortex	2.39	2.65	0.49	2.94	3.58	2.18[c]
f_P	8%	5.3%	0.8%	ND	16.0%	6.8%[d]
Mean V_T/f_P	0.50	0.76	0.86	ND	0.39	0.55

[a]Gunn et al., 2011.
[b]Sanabria-Bohorquez et al., 2012.
[c]Joshi et al., 2015.
[d]unpublished data, n = 10, ND: not determined.

and faster kinetics than [^{11}C]GSK931145. Regional time activity curves were well described by the two-tissue compartment model, and kinetic parameters were reliably estimated for both radiotracers. Higher regional V_T and BP_{ND} values were found for [^{18}F]MK-6577 than [^{11}C]GSK931145. Based on these analyses, [^{18}F]MK-6577 was judged to be a superior GlyT1 radiotracer and thus was chosen for use to image GlyT1 in healthy human subjects and patients with schizophrenia in our Center.

CONCLUSION

Both [^{11}C]GSK931145 and [^{18}F]MK-6577 are potent and selective GlyT1 radiotracers suitable for occupancy studies, where changes in transporter availability tend to be large. In comparison, [^{18}F]MK-6577 appears to be a superior radiotracer with higher brain uptake, faster kinetics, and higher specific binding signals. These favorable characteristics, coupled with the better counting statistics of the F-18 radiolabel, will allow for more reliable estimates of outcome measures. Hence [^{18}F]MK-6577 is considered the radiotracer of choice for the investigation of GlyT1 in neuropsychiatric disorders, where alterations may be subtle and small in magnitude. The availability of an F-18 labeled tracer such as [^{18}F]MK-6577 will also facilitate its wider use as it can be produced in one central location and transported off site for imaging applications to enable multi-center clinical trials, and more sites are capable of implementing F-18 tracers compared to C-11 chemistry.

ACKNOWLEDGMENTS

The authors gratefully acknowledge the expert technical assistance from the staff of the Yale PET Center. They have no conflict of interest to declare.

REFERENCES

Castner SA, Murthy NV, Ridler K, Herdon H, Roberts BM, Weinzimmer DP, Huang Y, Zheng MQ, Rabiner EA, Gunn RN, Carson RE, Williams GV, Laruelle M. 2014. Relationship between glycine transporter 1 inhibition as measured with positron emission tomography and changes in cognitive performances in non-human primates. Neuropsychopharmacology 39:2742–2749.

Cubelos B, Gimenez C, Zafra F. 2005. Localization of the GLYT1 glycine transporter at glutamatergic synapses in the rat brain. Cereb Cortex 15:448–459.

Cunningham VJ, Rabiner EA, Slifstein M, Laruelle M, Gunn RN. 2010. Measuring drug occupancy in the absence of a reference region: The Lassen plot re-visited. J Cereb Blood Flow Metab 30: 46–50.

Fuchigami T, Takano A, Gulyas B, Jia Z, Finnema SJ, Andersson JD, Nakao R, Magata Y, Haratake M, Nakayama M, Halldin C. 2012. Synthesis and evaluation of 2-chloro N-[(S)-{(S)-1-[^{11}C]methylpiperidin-2-yl} (phenyl)methyl]3-trifluoromethyl-benzamide ([^{11}C]N-methyl-SSR504734) as a PET radioligand for glycine transporter 1. EJNMMI Res 2:37.

Gunn RN, Murthy V, Catafau AM, Searle G, Bullich S, Slifstein M, Ouellet D, Zamuner S, Herance R, Salinas C, Pardo-Lozano R, Rabiner EA, Farre M, Laruelle M. 2011. Translational characterization of [^{11}C]GSK931145, a PET ligand for the glycine transporter type 1. Synapse 65:1319–1332.

Guo Q, Owen DR, Rabiner EA, Turkheimer FE, Gunn RN. 2014. A graphical method to compare the in vivo binding potential of PET radioligands in the absence of a reference region: Application to [^{11}C]PBR28 and [^{18}F]PBR111 for TSPO imaging. J Cereb Blood Flow Metab 34:1162–1168.

Hamill TG, Eng W, Jennings A, Lewis R, Thomas S, Wood S, Street L, Wisnoski D, Wolkenberg S, Lindsley C, Sanabria-Bohorquez SM, Patel S, Riffel K, Ryan C, Cook J, Sur C, Burns HD, Hargreaves R. 2011. The synthesis and preclinical evaluation in rhesus monkey of [^{18}F]MK-6577 and [^{11}C]CMPyPB glycine transporter 1 positron emission tomography radiotracers. Synapse 65: 261–270.

Innis RB, Cunningham VJ, Delforge J, Fujita M, Gjedde A, Gunn RN, Holden J, Houle S, Huang SC, Ichise M, Iida H, Ito H, Kimura Y, Koeppe RA, Knudsen GM, Knuuti J, Lammertsma AA, Laruelle M, Logan J, Maguire RP, Mintun MA, Morris ED, Parsey R, Price JC, Slifstein M, Sossi V, Suhara T, Votaw JR, Wong DF, Carson RE. 2007. Consensus nomenclature for in vivo imaging of reversibly binding radioligands. J Cereb Blood Flow Metab 27:1533–1539.

Javitt DC. 2012. Glycine transport inhibitors in the treatment of schizophrenia. Handb Exp Pharmacol 213:367–399.

Joshi AD, Sanabria-Bohorquez SM, Bormans G, Koole M, De Hoon J, Van Hecken A, Depre M, De Lepeleire I, Van Laere K, Sur C, Hamill TG. 2015. Characterization of the novel GlyT1 PET tracer [^{18}F]MK-6577 in humans. Synapse 69:33–40.

Martin-Facklam M, Pizzagalli F, Zhou Y, Ostrowitzki S, Raymont V, Brasic JR, Parkar N, Umbricht D, Dannals RF, Goldwater R, Wong DF. 2013. Glycine transporter type 1 occupancy by bitopertin: A positron emission tomography study in healthy volunteers. Neuropsychopharmacology 38:504–512.

Passchier J, Gentile G, Porter R, Herdon H, Salinas C, Jakobsen S, Audrain H, Laruelle M, Gunn RN. 2010. Identification and evaluation of [^{11}C]GSK931145 as a novel ligand for imaging the type 1 glycine transporter with positron emission tomography. Synapse 64:542–549.

Sanabria-Bohorquez SM, Joshi AD, Holahan M, Daneker L, Riffel K, Williams M, Li W, Cook JJ, Hamill TG. 2012. Quantification of the glycine transporter 1 in rhesus monkey brain using [^{18}F]MK-6577 and a model-based input function. Neuroimage 59:2589–2599.

Strzelecki D, Podgorski M, Kaluzynska O, Gawlik-Kotelnicka O, Stefanczyk L, Kotlicka-Antczak M, Gmitrowicz A, Grzelak P. 2015. Supplementation of antipsychotic treatment with sarcosine - GlyT1 inhibitor - causes changes of glutamatergic ^{1}NMR spectroscopy parameters in the left hippocampus in patients with stable schizophrenia. Neurosci Lett 606:7–12.

Toyohara J, Ishiwata K, Sakata M, Wu J, Nishiyama S, Tsukada H, Hashimoto K. 2011. In vivo evaluation of carbon-11-labelled non-sarcosine-based glycine transporter 1 inhibitors in mice and conscious monkeys. Nucl Med Biol 38:517–527.

Wong DF, Ostrowitzki S, Zhou Y, Raymont V, Hofmann C, Borroni E, Kumar A, Parkar N, Brasic JR, Hilton J, Dannals RF, Martin-Facklam M. 2013. Characterization of [^{11}C]RO5013853, a novel PET tracer for the glycine transporter type 1 (GlyT1) in humans. Neuroimage 75:282–290.

Xia Y, Zheng MQ, Holden D, Lin SF, Kapinos M, Ropchan J, Gallezot JD, Huang Y, Carson RE. 2015. Measurement of B_{max} and K_d with the glycine transporter 1 radiotracer [^{18}F]-MK6577 using a novel multi-infusion paradigm. J Cereb Blood Flow Metab 35:2001–2009.